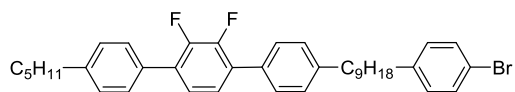


Supplementary Information for Parsouzi et al, "Pretransitional behavior of viscoelastic parameters at the uniaxial to twist-bend nematic phase transition in flexible n-mers"

A. Synthesis of the trimer and tetramer

4-(9-(4-bromophenyl)nonyl)-2',3'-difluoro-4''-pentyl-1,1':4',1''-terphenyl, 3



1,9-bis(4-bromophenyl)nonane **2** (7.60 g, 17.3 mmol) and (2,3-difluoro-4'-pentyl-[1,1'-biphenyl]-4-yl)boronic acid **1** (1.76 g, 5.8 mmol) were dissolved in tetrahydrofuran (100 mL) and a solution of aqueous sodium carbonate (2 mol.dm⁻³, 40 mL) added. Dry nitrogen gas was bubbled through the resulting solution for 20 minutes, Pd(PPh₃)₄ (0.19 g, 0.22 mmol, 4 mol%) added in one portion and the reaction subsequently heated to 90°C for 16 hours under reflux conditions. After cooling to ambient temperature, water (100 mL) was added and the mixture extracted with dichloromethane (3 x 100 mL). The combined organic extracts were washed with water (2 x 100 mL) and dried over anhydrous MgSO₄ (s). After removal of the dessicant by filtration, the organics were concentrated *in vacuo* and the product isolated by column chromatography (Silica gel, eluent: Hexane / CH₂Cl₂, 95:5). Hot recrystallisation from a mixture of ethanol/ethyl acetate gave the product **3** as off-white crystals. Yield 2.81g, 79%

δ_{H} (400MHz; CD₂Cl₂) 7.53-7.48 (m, 4H), 7.39 (d, ³J(H-H) = 8.3 Hz, 2H), 7.33-7.25 (m, 6H), 7.07 (d, ³J(H-H) = 8.7 Hz, 2H), 2.72-2.63 (m, 4H), 2.59 (t, ³J(H-H) = 7.8 Hz, 2H), 1.72-1.53 (m, 6H), 1.43-1.26 (m, 14H), 0.92 (t, ³J(H-H) = 6.9 Hz, 3H)

δ_{C} (100MHz; CD₂Cl₂) 148.89 (dd, ¹J(C-F) = 249.5 Hz, ²J(C-F) = 15.4 Hz), 143.74 (d, J(C-F) = 1.9 Hz), 142.54 (s), 132.24 (s), 131.52 (s), 130.64 (s), 130.00-129.80 (m), 129.09 (s), 129.04 (s), 125.07 (s), 119.40 (s), 36.00 (s), 35.64 (s), 31.94 (s), 31.86(s), 31.73 (s), 31.57 (s), 29.85 (s), 29.80 (s), 29.70 (s), 29.54 (s) 22.96 (s), 14.22 (s)

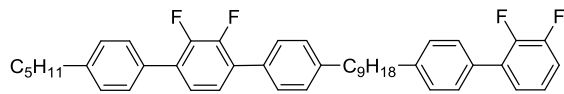
δ_{F} (376MHz; CD₂Cl₂) -144.19 (s)

MS (APCI) *m/z* 617.3 (M+H)⁺

HRMS : calculated for C₃₈H₄₄BrF₂ : 617.2594, found 617.2591

anal. calculated for C₃₈H₄₃BrF₂: C 73.89, H 7.02; found: C 74.12, H 7.17

4-(9-(2',3'-difluoro-[1,1'-biphenyl]-4-yl)nonyl)-2',3'-difluoro-4''-pentyl-1,1':4',1''-terphenyl, 4



2,3-difluorophenyl boronic acid (1.53 g, 9.7 mmol) and **3** (2.0 g, 3.2 mmol) were dissolved in THF (50 mL) and a solution of aqueous sodium carbonate (2 mol.dm⁻³, 10 mL) added. Dry nitrogen gas was bubbled through the resulting solution for 15 mins., Pd(PPh₃)₄ (130 mg, 0.1 mmol, 3 mol%) added in one portion and the reaction subsequently heated to 90°C for 16 hours under reflux conditions. After cooling to ambient temperature, water (100 mL) was added and the mixture extracted with diethyl ether (3 x 75 mL). The combined organic extracts were washed with water (2 x 100 mL) and dried over anhydrous MgSO₄ (s). After removal of the dessicant by filtration, the organics were concentrated *in vacuo* and the product isolated by column chromatography (Silica gel, eluent: Hexane / CH₂Cl₂, 9:1). Hot recrystallisation from a mixture of ethanol/ethyl acetate gave **4** as white crystals. Yield 1.85 g, 88 %

δ_{H} (400MHz; CD₂Cl₂) 7.53-7.48 (m, 4H), 7.48-7.43 (m, 2H), 7.33-7.25 (m, 8H), 7.24-7.15 (m, 3H), 2.70-2.63 (m, 6H), 1.71-1.60 (m, 6H), 1.43-1.29 (m, 14H), 0.94-0.89 (m, 3H)

δ_{C} (100MHz; CD₂Cl₂) 151.50 (dd, ¹J(C-F) = 246.6 Hz, ²J(C-F) = 13.5 Hz), 148.80 (dd, ¹J(C-F) = 249.5 Hz, ²J(C-F) = 15.4 Hz), 148.27 (dd, ¹J(C-F) = 248.5 Hz, ²J(C-F) = 13.5 Hz), 143.74 (s), 132.23 (s), 131.64 (d, ³J(C-F) = 9.6 Hz), 129.95-129.70 (m), 129.08 (s), 129.03 (s), 125.82-125.68 (m), 125.16-124.96 (m), 124.65-124.45 (m), 116.06 (d, ²J(C-F) = 17.3 Hz), 36.00 (s), 31.94 (s), 31.87 (s), 31.57 (s), 29.85 (s), 29.71 (s), 22.95 (s), 14.22 (s)

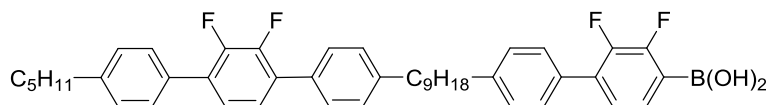
δ_{F} (376MHz; CD₂Cl₂) -139.02 — -139.15 (m, 1F), -144.20 (s, 2F), -144.69 — -144.81 (m, 1F)

MS (APCI) *m/z* 651.4 (M+H)⁺

HRMS : calculated for C₄₄H₄₇F₄ : 651.3614, found 651.3616

anal. calculated for C₄₄H₄₆F₄: C 81.20, H 7.12; found: C 80.99, H 7.12

(4'-(9-(2',3'-difluoro-4''-pentyl-[1,1':4',1''-terphenyl]-4-yl)nonyl)-2,3-difluoro-[1,1'-biphenyl]-4-yl)boronic acid, 5



Compound **4** (1.80 g, 2.77 mmol) was dissolved in anhydrous THF (40 mL) under a dry N₂ atmosphere and the resulting solution cooled to -78°C. ⁿBuLi (2.5M in hexanes, 3.0 mmol, 1.2 mL) was added dropwise and the reaction was left to stir at -78°C for one hour before trimethyl borate (0.94 mL, 8.3 mmol) was added in one portion and the reaction was allowed to rise slowly to ambient temperature over 16 hours. A solution of aqueous HCl (1M, 30mL) was added cautiously and the reaction stirred for two hours. The solvent was concentrated *in vacuo* until it became cloudy and the precipitate that subsequently formed was filtered off and washed with hexane (4 x 50 mL). Yield of white solid: 1.57 g, 82 %

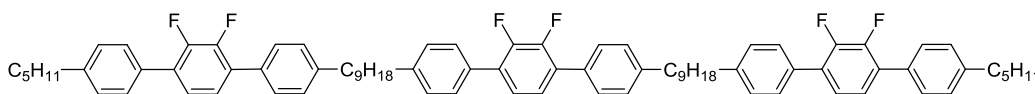
δ_{H} (400MHz; CD₂Cl₂) 7.62-7.55 (m, 1H), 7.54-7.45 (m, 6H), 7.35-7.23 (m, 9H), 5.12 (s, 1H), 5.11 (s, 1H), 2.67 (t, ³J(H-H) = 7.8 Hz, 6H), 1.72-1.59 (m, 6H), 1.45-1.25 (m, 14H), 0.95-0.88 (m, 3H)
 δ_{C} (100MHz; CD₂Cl₂) 156.25 (dd, ¹J(C-F) = 243.7 Hz, ²J(C-F) = 12.5 Hz), 148.88 (dd, ¹J(C-F) = 249.5 Hz, ²J(C-F) = 15.4 Hz), 147.83 (dd, ¹J(C-F) = 252.4 Hz, ²J(C-F) = 13.5 Hz), 144.20 (s), 143.74 (s), 134.45 (d, ³J(C-F) = 9.6 Hz), 132.24 (s), 132.00-131.85 (m), 130.85-130.65 (m), 129.95-129.75 (m), 129.08 (s), 129.03 (s), 125.80 (br s), 125.15-124.95 (m), 36.01 (s), 31.94 (s), 31.86 (s), 31.83 (s), 31.56 (s), 29.84 (s), 29.69 (s), 22.95 (s), 14.21 (s)

δ_{F} (376MHz; CD₂Cl₂) -135.69 — -135.83 (m, 1F), -144.22 (s, 2F), -145.91 (dd, ³J(F-F) = 21.7 Hz, ⁴J(F-H) = 5.8 Hz, 1F)

MS (APCI) *m/z* 720.4 (M+H)⁺ (Ethylene glycol adduct)

HRMS : calculated for C₄₆H₅₀O₂F₄¹⁰B : 720.3876, found 720.3871

4'',4''''-((2',3'-difluoro-[1,1':4',1''-terphenyl]-4,4''-diyl)bis(nonane-9,1-diyl))bis(2',3'-difluoro-4-pentyl-1,1':4',1''-terphenyl), **6**



Compound **5** (240 mg, 0.35 mmol) and **3** (427 mg, 0.69 mmol) were dissolved in THF (40 mL) and a solution of aqueous sodium carbonate (2 mol.dm⁻³, 10 mL) added. Dry nitrogen gas was bubbled through the resulting solution for 30 minutes, Pd(PPh₃)₄ (37 mg, 9 mol%) added in one portion and the reaction subsequently heated to 90°C for 24 hours under reflux conditions. Upon cooling to ambient temperature, an off-white precipitate formed. Water (50 mL) and CH₂Cl₂ (50 mL) were added and the organic layer separated. This was slowly concentrated *in vacuo* until it exhibited a cloudy appearance. The solution was reformed by addition of a small amount of CH₂Cl₂

(3 mL approx.) and acetone (20mL) subsequently added. White crystals formed over a period of two hours and were collected by filtration before being washed thoroughly with acetone. Yield of white crystals: 313 mg, 76 %

δ_{H} (400 MHz, CDCl_3) δ 7.53-7.48 (m, 12H), 7.32-7.27 (m, 12H), 7.25-7.22 (m, 6H), 2.66 (t, $^3\text{J}(\text{C}-\text{H}) = 7.8$ Hz, 12H), 1.73-1.61 (m, 12H), 1.43-1.28 (m, 28H), 0.92 (t, $^3\text{J}(\text{C}-\text{H}) = 7.3$ Hz, 6H)

δ_{C} (100MHz; CDCl_3) 148.62 (dd, $^1\text{J}(\text{C}-\text{F}) = 250.5$ Hz, $^2\text{J}(\text{C}-\text{F}) = 16.4$ Hz), 143.21 (s), 132.12 (s), 129.72-129.52 (m), 128.83 (s), 124.80-124.60 (m), 35.87 (s), 31.71 (s), 31.56 (s), 31.26 (s), 29.63 (s), 29.48 (s), 22.72 (s), 14.21 (s)

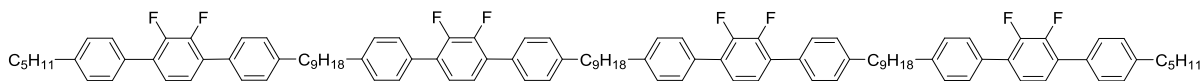
δ_{F} (376MHz; CDCl_3) -143.22 (s)

MS (APCI) m/z 1189.7 (M+H)⁺

HRMS : calculated for $\text{C}_{82}\text{H}_{89}\text{F}_6$: 1187.6868, found 1187.6866

anal. calculated for $\text{C}_{82}\text{H}_{88}\text{F}_6$: C 82.93, H 7.47; found: C 82.92, H 7.52

1,9-bis(4''-(9-(2',3'-difluoro-4''-pentyl-[1,1':4',1''-terphenyl]-4-yl)nonyl)-2',3'-difluoro-[1,1':4',1''-terphenyl]-4-yl)nonane, 7



Compound **5** (525 mg, 0.76 mmol) and **2** (150 mg, 0.34 mmol) were dissolved in THF (40mL) at 50°C and $\text{Na}_2\text{CO}_3(\text{aq})$ (2 mol.dm⁻³, 10 mL) added. Nitrogen was bubbled through the resulting solution for 30 mins and then $\text{Pd}(\text{PPh}_3)_4$ added (40 mg, 0.03 mmol, 10 mol%). The reaction was heated under reflux conditions to 90° under nitrogen for 15hrs. Upon cooling to ambient temperature, an off-white precipitate was formed. This was filtered off and washed sequentially with water (10 x 50 mL) and acetone (10 x 50 mL). Yield of **7**: 305 mg, 56 %

δ_{H} (400 MHz, CD_2Cl_2) δ 7.55-7.47 (m, 16H), 7.35-7.24 (m, 24H), 2.72-2.63 (m, 16H), 1.73-1.62 (m, 16H), 1.44-1.29 (m, 38H), 0.95 - 0.88 (m, 6H)

δ_{C} (100MHz; CDCl_3) 148.65 (dd, $^1\text{J}(\text{C}-\text{F}) = 250.5$ Hz, $^2\text{J}(\text{C}-\text{F}) = 15.4$ Hz), 143.22 (s), 132.14 (s), 129.71 - 129.53 (m), 128.83 (br s), 124.70 - 124.56 (m), 35.87 (s), 31.72 (s), 31.55 (s), 31.26 (s), 29.63 (s), 29.49 (s), 22.72 (s), 14.20 (s)

δ_{F} (376MHz; CD_2Cl_2) -143.23 (s)

MS (APCI) m/z 1577.9 (M+H)⁺

HRMS : calculated for $\text{C}_{109}\text{H}_{117}\text{F}_8$: 1577.9028, found 1577.9026

anal. calculated for C₁₀₉H₁₁₆F₈: C 82.96, H 7.41; found: C 82.82, H 7.47

Detailed NMR and high resolution mass spectra of the intermediate and final compounds are provided in the Appendix at the end of the ESI.

B. DSC results on the dimer, trimer and tetramer

The transition temperatures below were determined on heating, and differ somewhat from those measured optically on cooling, which are reported in the main text. The differences are attributable to different thermometer calibrations, differences in the thermal characteristics of the heat stages, and differences in placement of the thermometers relative to the sample volume probed (i.e., thermal gradients), as well as possible heating/cooling hysteresis. We note that the transitions temperatures and thermal values for DTC5C9 are systematically shifted when compared to recent MDSC data¹ obtained with heating rates of 0.01 to 0.04 K.

DTC5C9 (797.08 gmol⁻¹) **Cr 95 N_{TB} 126 N 164 Iso**

	ΔH Cr-N _{TB}	ΔH N _{TB} -N	ΔH N-Iso
$\Delta H / \text{J.g}^{-1}$	59.1	0.03	0.76
$\Delta H / \text{kJ.mol}^{-1}$	47.1	0.02	0.61
$\Delta S / \text{J.mol}^{-1}.\text{K}^{-1}$	127.6	0.06	1.38

C9C9 trimer (1187.60 gmol⁻¹) **Cr 127 N_{TB} 149 N 188 Iso**

	ΔH Cr-N _{TB}	ΔH N _{TB} -N	ΔH N-Iso
$\Delta H / \text{J.g}^{-1}$	42.4	0.49	3.12
$\Delta H / \text{kJ.mol}^{-1}$	50.4	0.58	3.71
$\Delta S / \text{J.mol}^{-1}.\text{K}^{-1}$	126.5	1.39	7.93

C9C9C9 tetramer (1578.11 gmol⁻¹) **Cr 142 N_{TB} 167 N 204 Iso**

	ΔH Cr-N _{TB}	ΔH N _{TB} -N	ΔH N-Iso
$\Delta H / \text{J.g}^{-1}$	49.8	1.30	2.22
$\Delta H / \text{kJ.mol}^{-1}$	78.5	2.05	3.50
$\Delta S / \text{J.mol}^{-1}.\text{K}^{-1}$	189.3	4.71	7.37

Table S1: Enthalpy and entropy changes at the I – N, N – N_{TB}, and N_{TB} – Cr transitions in the studied n-mers.

DSC scans

Trimer

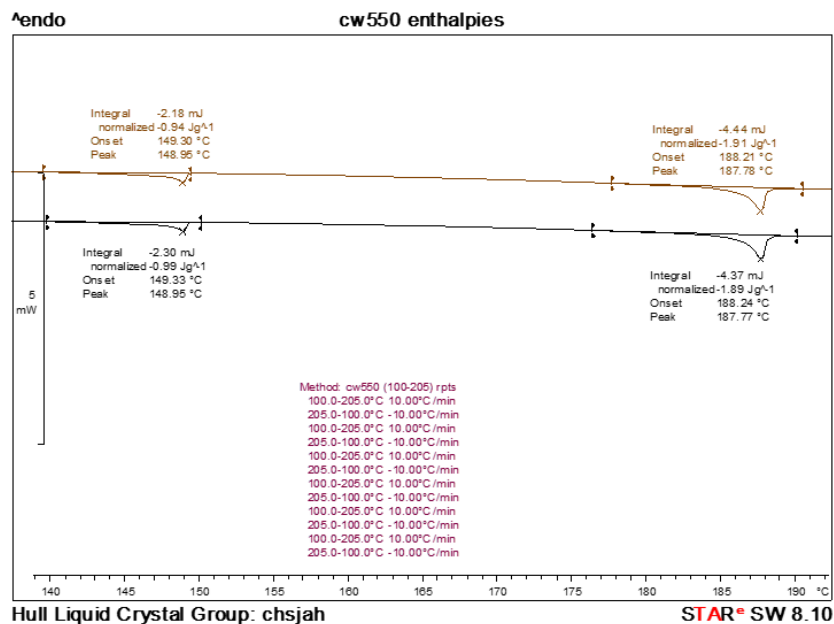
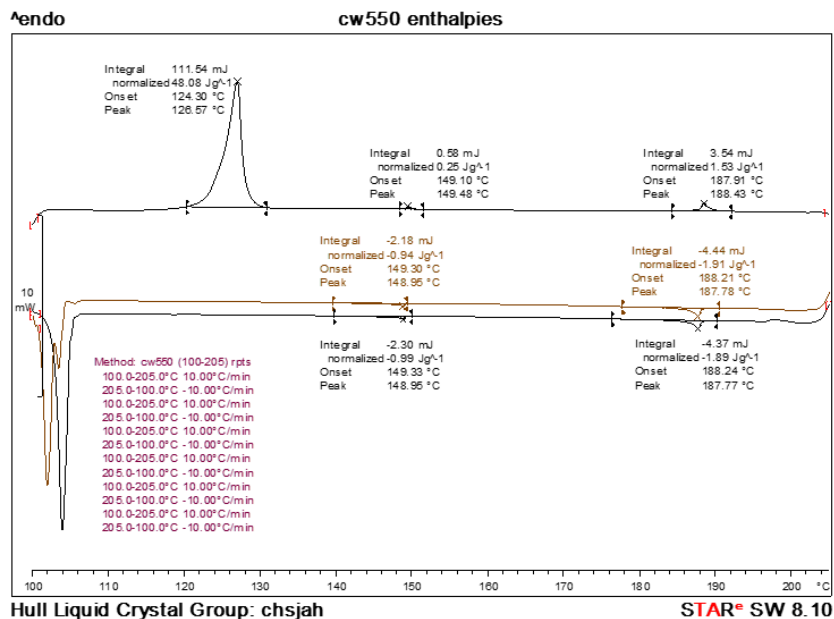


Figure S1: Top: DSC traces for the studied trimer (“CW550”), including first heating and first and second cooling scans. Bottom: Traces for first and second cooling scans, magnified (140 – 200 °C).

Tetramer

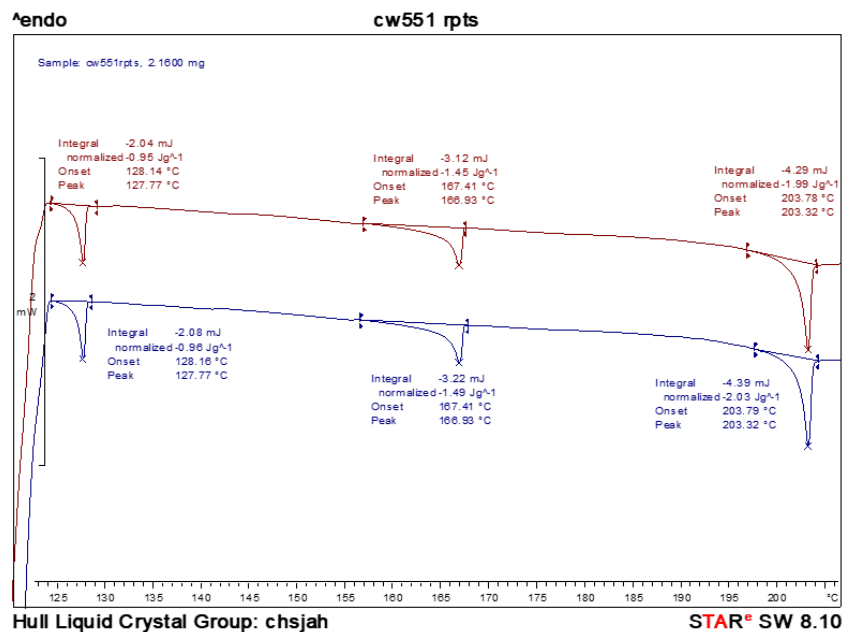
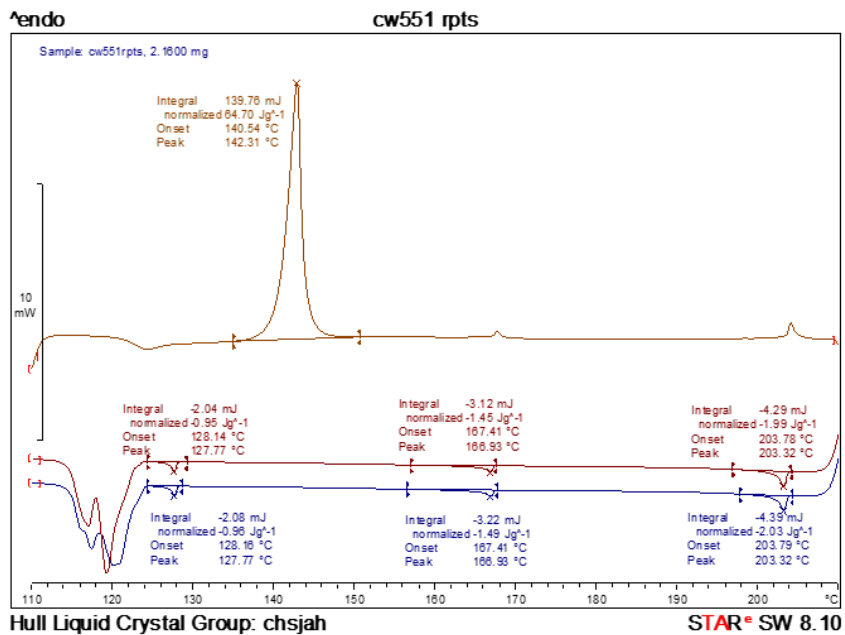


Figure S2: Top: DSC traces for the studied tetramer (“CW551”), including first heating and first and second cooling scans. Bottom: Traces for first and second cooling scans, magnified (120 – 210 °C).

Dimer

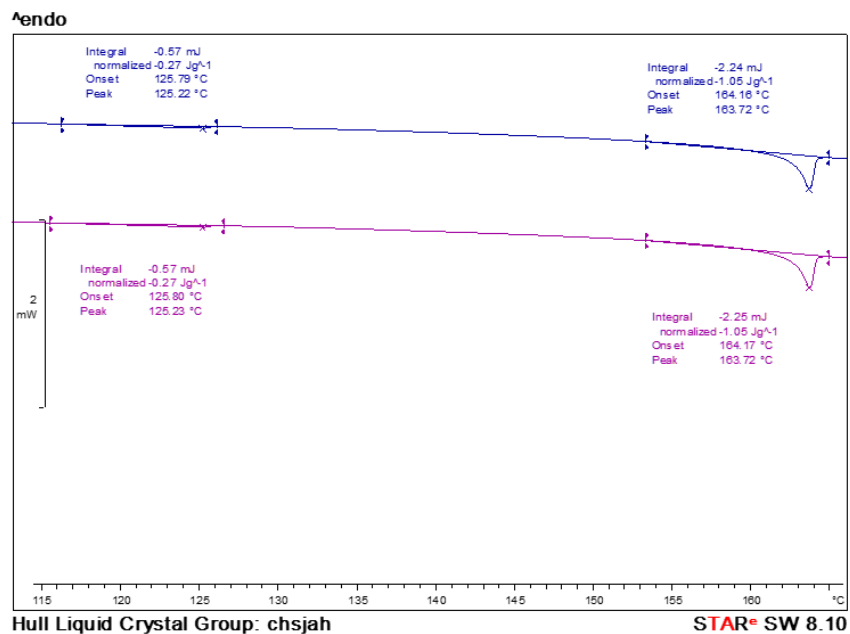
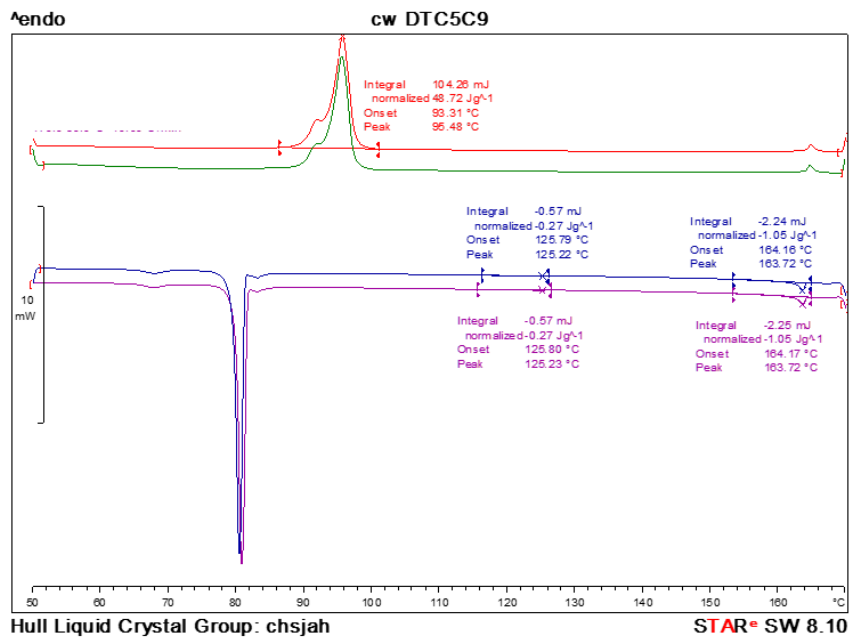


Figure S3: Top: DSC traces for the studied dimer (“DTC5C9”), including first and second heating and cooling scans. Bottom: Traces for first and second cooling scans, magnified (115 – 165 °C).

C. Sample SAXS lineshapes

The following figures present typical small angle x-ray scattering data collected in the N and N_{TB} phases of the studied n-mers at the CMS beamline at NSLS2, Brookhaven National Laboratory, USA. Azimuthal averages of the raw scattering data (recorded on an area detector) are plotted against the magnitude of the scattering vector.

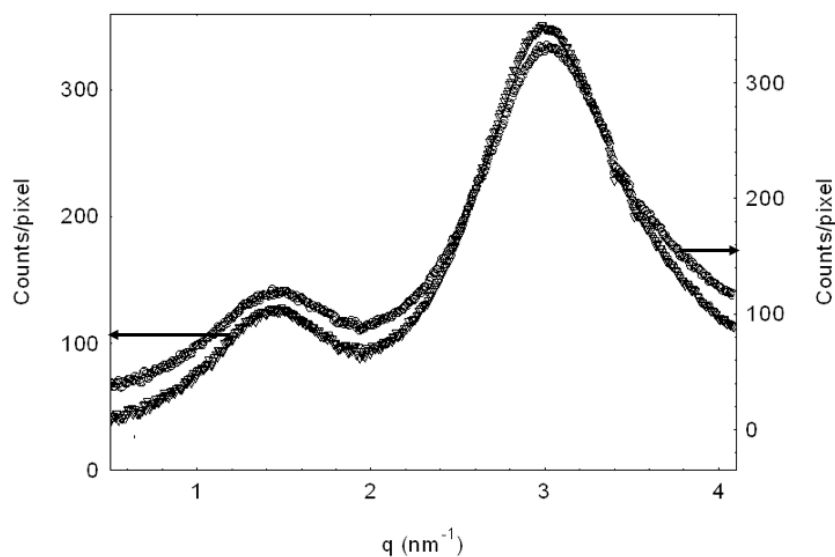


Figure S4: Typical SAXS lineshapes for the studied dimer in the N phase at $T - T_{NTB} = 1^\circ\text{C}$ (left axis) and N_{TB} phase at $T - T_{NTB} = -1^\circ\text{C}$ (right axis).

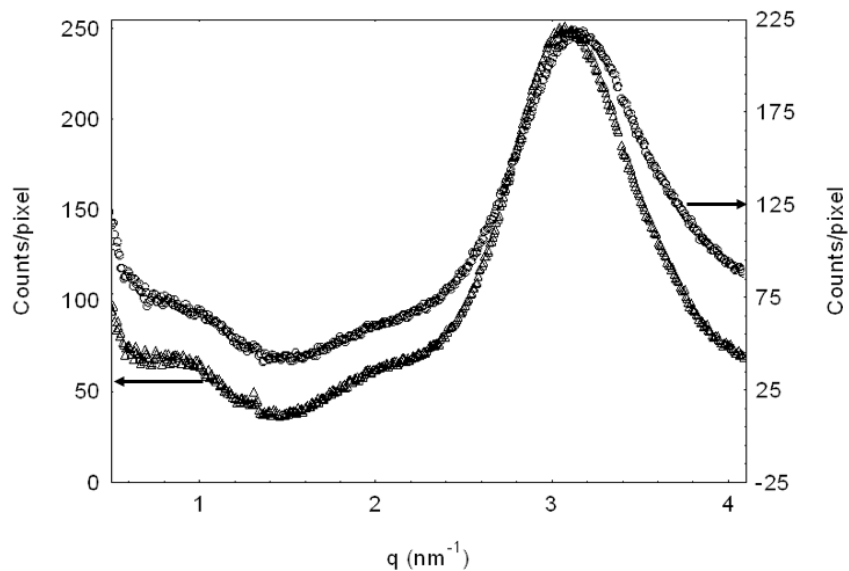


Figure S5: Typical SAXS lineshapes for the studied trimer in the N phase at $T - T_{NTB} = 2^\circ\text{C}$ (left axis) and N_{TB} phase at $T - T_{NTB} = -2^\circ\text{C}$ (right axis).

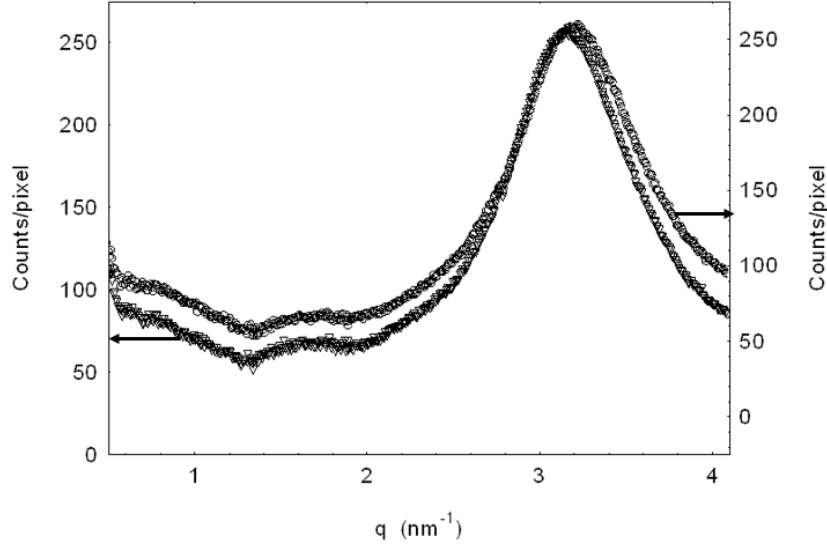


Figure S6: Typical SAXS lineshapes for the studied tetramer in the N phase at $T - T_{NTB} = 1^\circ\text{C}$ (left axis) and N_{TB} phase at $T - T_{NTB} = -2^\circ\text{C}$ (right axis).

D. Light scattering measurements

For our light scattering measurements, we employed three scattering geometries, shown schematically in Fig. S7. In each case, the incident light propagated along the cell normal and was polarized perpendicular to the scattering plane, while the scattered light collected at specific angles off the cell normal was polarized parallel to the plane.

In *geometry 1*, the average director is oriented perpendicular to the scattering plane. Pure splay and pure twist contribute to the light scattering for arbitrary scattering angle θ . Choosing θ to be $\theta_m = \sin^{-1}\left(n_o \sqrt{1 - n_o^2 / n_e^2}\right)$, we can isolate pure splay². To calculate this angle for different temperatures in the N phase of the dimer and trimer, we measured the refractive indices n_e and n_o separately as functions of T by the wedge cell technique³. For the tetramer, we used the measured Δn and took $n_o = 1.5$, which is extrapolated from the average values of n_o in the nematic phase of the dimer and trimer (1.44 and 1.47, respectively).

In *geometry 3*, the equilibrium director lies in the scattering plane. In this case, selecting $\theta = \theta_m$ (the same “magic” angle as in *geometry 1*) sets the scattering vector (and fluctuation wavevector) parallel to \hat{n} , which corresponds to pure bend fluctuations.

Finally, in *geometry 2* the director is oriented parallel to the scattering plane, which, for arbitrary θ , selects the twist-bend normal mode of the director fluctuations. The intensity scattered

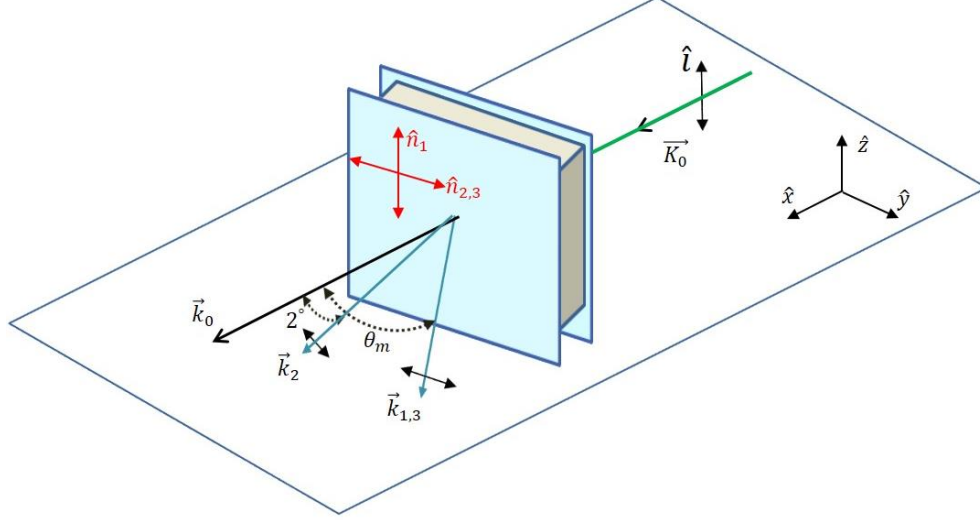


Figure S7: Scattering geometries utilized in our DLS measurements. Subscripts 1 (3) denote conditions for collection of pure splay (bend) scattering, where the equilibrium director \hat{n} is oriented perpendicular (parallel) to the scattering plane, and the scattering angle is set to the “magic” angle (see text) for normal incidence. Almost pure twist scattering (subscript 2) is selected when \hat{n} lies in the scattering plane and the laboratory scattering angle is set to a small value (2° in our case). In all three cases, the incident and scattered light polarizations (displayed by double-ended arrows) are normal and parallel to the scattering plane, respectively.

from this mode is $I \propto \frac{k_B T}{K_{22} q_\perp^2 + K_{33} q_\parallel^2}$, where q_\perp (q_\parallel) is the component of the scattering vector perpendicular (parallel) to the average \hat{n} . The laboratory scattering angle is set to a low value of $\theta = 2^\circ$, for which $\frac{q_\perp^2}{q_\parallel^2} \approx 15 - 20 \gg 1$. Since n-mers that form the N_{TB} phase have $K_{22} \geq K_{33}$ (and $K_{22} \gg K_{33}$ approaching the transition), the condition $K_{22} q_\perp^2 \gg K_{33} q_\parallel^2$ applies, and thus the intensity at the small angle is contains only a few percent contribution from the bend elastic constant.

E. Analysis of the “coarse-grained” model for the N to N_{TB} transition

In direct analogy to the N to SmA^* transition, Dozov and Meyer^{4,5} expand the Landau-deGennes free energy density describing the transition from the uniaxial N to pseudo-layered N_{TB} phase as

$$\begin{aligned}
 f_{N-N_{TB}}^{CG} = & \frac{a}{2} |\sigma|^2 + \frac{c}{4} |\sigma|^4 + \frac{\gamma_\parallel}{2} |\nabla_\parallel \sigma|^2 + \frac{\gamma_\perp}{2} |(\vec{\nabla}_\perp - iq_0 \vec{N}_\perp) \sigma|^2 + \frac{K_{11}^N}{2} (\vec{\nabla} \cdot \hat{N})^2 \\
 & + \frac{K_{22}^N}{2} (\hat{N} \cdot \vec{\nabla} \times \hat{N} - t_0)^2 + \frac{K_{33}^N}{2} (\hat{N} \times \vec{\nabla} \times \hat{N})^2
 \end{aligned} \tag{S1}$$

Here $\sigma = \sin \beta e^{i\delta\phi}$ is the analog of the smectic order parameter, β is the tilt angle of the local director \hat{n} away from the average heliconical axis \hat{z} , and $\delta\phi$ is the deviation of the phase of the nematic director \hat{n} from its equilibrium value in the heliconical N_{TB} structure. The quantity $\hat{N} = (\vec{N}_\perp, \sqrt{1 - N_\perp^2})$ is the coarse-grained director, which is equivalent to the heliconical axis (or pseudo-layer normal) in the N_{TB} phase and to the uniaxial director \hat{n} in the N phase. The subscripts \parallel (\perp) refer to directions parallel (perpendicular) to the equilibrium pseudo-layer normal \hat{z} , while the superscript N in Eq. (S1) indicates orientational elastic constants that apply to the coarse-grained director. Since the molecules are achiral, there is no intrinsic twist, and $t_0 = 0$, in the N phase.

According to the ‘‘elastic instability’’ model, the local free energy density describing the N – N_{TB} transition is given by⁶

$$f_{N-N_{TB}}^{loc} = \frac{K_{11}}{2} (\vec{\nabla} \cdot \hat{n})^2 + \frac{K_{22}}{2} [\hat{n} \cdot (\vec{\nabla} \times \hat{n})]^2 + \frac{K_{33}}{2} [\hat{n} \times (\vec{\nabla} \times \hat{n})]^2 + \frac{C_1}{4} \left[\frac{d^2(n_i n_j)}{dz^2} \right]^2 + \frac{C_2}{2} \left[\frac{d^2(n_z n_i)}{dz^2} \right]^2 + \frac{C_3}{4} \left[\frac{d^2(n_z^2)}{dz^2} \right]^2 \quad (S2)$$

where \hat{n} is the nematic director, and summation on the indices i, j inside square brackets is implied. The bend elastic constant K_{33} has temperature dependence $K_{33} = k_{33}^0 (T - T^*)$ and becomes negative if $T < T^*$, which favors a spontaneous bend. Eq. (S2) includes higher-order gradients in \hat{n} (characterized by positive elastic constants C_i) that stabilize the energy when this occurs.

Let us consider the relation between the coefficients in Eqs. (S1) and (S2). Above the N – N_{TB} transition, we express the order parameter σ in a fluctuating pseudo-layer domain as $\sigma = \delta\beta \exp(iq_0 z)$, where q_0 is the wavenumber characterizing the heliconical structure in the domain, and $\delta\beta$ is a fluctuation away from the equilibrium value $\beta = 0$ in the N phase. Then, substituting this expression for σ and $\hat{N} = \hat{n}$ into Eq. (S1), we obtain $f_{N-N_{TB}}^{CG}$ in terms of $\delta\beta$ and \hat{n} . Next, using the results obtained by Dozov and Meyer^{4,5} from averaging the ‘‘local’’ free-energy density $f_{N-N_{TB}}^{loc}$ over the pitch in a pretransitional N_{TB} domain, we find that the coefficients in

$f_{N-N_{TB}}^{CG}$ are related to those in $f_{N-N_{TB}}^{loc}$ as

$$\begin{aligned} a &= \gamma_\parallel q_0^2 = (K_{33} + C q_0^2) q_0^2 \\ c &= (K_{22} - K_{33}) q_0^2 \\ \gamma_\perp &= (K_{11} + K_{22}) / 2 \\ K_{11}^N &= K_{11}, K_{22}^N = K_{22}, K_{33}^N = K_{33} = k_{33}^0 (T - T^*) \end{aligned} \quad (S3)$$

where $C = C_1 + C_2$. Just a single higher order elastic constant remains if only the lowest order is kept in each term of Eq. (S2) when it is expanded in the cone angle $\delta\beta$ for a fluctuating (pretransitional) N_{TB} domain.

The wavenumber q_0 of the twist-bend modulation appears as an independent parameter in Eqs. (S3). In the N phase, it is not possible to derive an expression for q_0 by minimizing the extended local free energy. The minimum occurs when $\beta = 0$ for *any* q_0 . Physically, this means that the pitch p_0 in fluctuating N_{TB} domains in the N phase is not selected by the model; it must be considered a material parameter (with a possible temperature-dependence), which presumably matches at the transition temperature with the value on the low temperature side (i.e., in the N_{TB} phase)⁵.

Because $f_{N-N_{TB}}^{CG}$ (with $t_0 = 0$) is analogous term by term to the free energy density of the N–SmA transition, we may carry over standard results from analysis of the latter to discuss the “coarse-grained” N– N_{TB} transition. In particular, we may define anisotropic correlation lengths $\xi_{\perp} = \sqrt{\gamma_{\perp}/a}$ and $\xi_{\parallel} = \sqrt{\gamma_{\parallel}/a}$ to characterize the size of pretransitional pseudo-layered domains in the mean-field limit^{7,8}. Then using Eq. (S3), we obtain

$$\begin{aligned}\xi_{\perp} &= \sqrt{\frac{\gamma_{\perp}}{a}} = \sqrt{\frac{K_{11} + K_{22}}{2(K_{33} + Cq_0^2)}} \frac{1}{q_0} \\ \xi_{\parallel} &= \sqrt{\frac{\gamma_{\parallel}}{a}} = \frac{1}{q_0}\end{aligned}\tag{S4}$$

If q_0 is temperature-dependent, then near the N– N_{TB} transition (at $T = T_{NTB}$), we may write $q_0^2(T) \approx q_0^2(T_{NTB}) + q_0^{2'}(T_{NTB})(T - T_{NTB})$, where $q_0^2(T_{NTB})$ and $q_0^{2'}(T_{NTB})$ are the values of q_0^2 and its derivative at the transition. The transition occurs when coefficient a in Eq. (S3) passes through zero and becomes negative – i.e., $K_{33} + Cq_0^2 = 0$ at $T = T_{NTB}$, which gives $T_{NTB} = T^* - Cq_0^2(T_{NTB})/k_{33}^0$. Therefore, close to T_{NTB} , we can express ξ_{\perp} as:

$$\xi_{\perp} \approx \sqrt{\frac{K_{11} + K_{22}}{2[k_{33}^0 + Cq_0^{2'}(T_{NTB})]}} \frac{1}{q_0} (T - T_{NTB})\tag{S5}$$

Eqs. (S4) and (S5) are the results given in Eq. (2) of the main manuscript. Additionally,

$$a\xi_{\parallel} = (K_{33} + Cq_0^2)q_0 \approx [k_{33}^0 + Cq_0^{2'}(T_{NTB})](T - T_{NTB})q_0\tag{S6}$$

close to T_{NTB} , which is used in the discussion of orientational viscosities in the main text.

An alternative “local” model of the N–N_{TB} transition is the “polarization wave” model discussed by Shamid and Selinger⁹. The free energy density in this model is:

$$f_{N-NTB}^{loc} = \frac{K_{11}}{2} (\vec{\nabla} \cdot \hat{n})^2 + \frac{K_{22}}{2} [\hat{n} \cdot (\vec{\nabla} \times \hat{n})]^2 + \frac{K_{33}}{2} [\hat{n} \times (\vec{\nabla} \times \hat{n})]^2 - \lambda [\hat{n} \times (\vec{\nabla} \times \hat{n})] \cdot \vec{P} + \frac{\mu}{2} |\vec{P}|^2 + \frac{\nu}{4} |\vec{P}|^4 + \frac{\kappa}{2} (\vec{\nabla} \vec{P})^2 \quad (S7)$$

Here \vec{P} is a polarization field assumed to be perpendicular to the average nematic director, and $\mu = \mu'(T - T^*)$ is the only explicitly temperature-dependent coefficient.

In the N phase, fluctuations in the magnitude of \vec{P} are related to fluctuations of the heliconical tilt β by $\delta P = \frac{\lambda q_0}{\mu + \kappa q_0^2} \delta \beta$. Using this relation between δP and $\delta \beta$ to eliminate $|\vec{P}|$, we can obtain f_{N-NTB}^{loc} (Eq. (S5)) in terms of $\delta \beta$ and \hat{n} . The resulting expression can then be “coarse-grained” (averaged over a pitch) using the same procedure described by Dozov and Meyer for the “elastic instability” model. Connecting the coefficients in the result to those in Eq. (S1), we find

$$\xi_{\perp} = \sqrt{\frac{\gamma_{\perp}}{a}} = \sqrt{\frac{K_{11} + K_{22}}{2[K_{33} - \lambda^2 / (\mu + \kappa q_0^2)]}} \frac{1}{q_0} \approx \sqrt{\frac{K_{11} + K_{22}}{(2\mu' K_{33}^2 / \lambda^2)(T - T_{NTB})}} \frac{1}{q_0} \quad (S8)$$

$$\xi_{\parallel} = \sqrt{\frac{\gamma_{\parallel}}{a}} = \frac{1}{q_0}$$

The second expression for ξ_{\perp} is valid for T close to the transition temperature, which is given by $T_{NTB} = [T^* + \lambda^2 / (\mu' K_{33})] - \kappa [q_0(T_{NTB})]^2 / \mu'$. In Eq. (S8), K_{33} is the “bare” nematic bend constant, which has no significant temperature-dependence in the “polarization wave” theory.

From Eqs. (S4), (S5), and (S8), we see that the “elastic instability” and “polarization wave” models give similar results for the temperature dependence of the correlation lengths.

References

- 1 W. D. Stevenson, H. X. Zou, X. B. Zeng, C. Welch, G. Ungar and G. H. Mehl, *Phys. Chem. Chem. Phys.*, 2018, **20**, 25268–25274.
- 2 R. Schaetzing and J. D. Litster, *Adv. Liq. Cryst.*, 1979, **4**, 147–206.
- 3 J. Kedzierski, Z. Raszewski, M. A. Kojdecki, E. Kruszelnicki-Nowinowski, P. Perkowski, W. Piecek, E. Miszczyk, J. Zieliński, P. Morawiak and K. Ogrodnik, *Opto-electronics*

- Rev.*, 2010, **18**, 214–218.
- 4 C. Meyer and I. Dozov, *Soft Matter*, 2016, **12**, 574–580.
 - 5 I. Dozov and C. Meyer, *Liq. Cryst.*, 2017, **44**, 4–23.
 - 6 I. Dozov, *Eur. Lett.*, 2001, **56**, 247–253.
 - 7 P. G. de Gennes, *Solid State Commun.*, 1993, **88**, 1039–1042.
 - 8 P. G. de Gennes and J. Prost, *The Physics of Liquid Crystals*, Clarendon Press, Oxford, UK, 2nd edn., 1993.
 - 9 S. M. Shamid, S. Dhakal and J. V. Selinger, *Phys. Rev. E*, 2013, **87**, 052503.

Appendix 1: ^1H , ^{13}C , ^{19}F and HRMS spectra for intermediates and final trimer and tetramer products

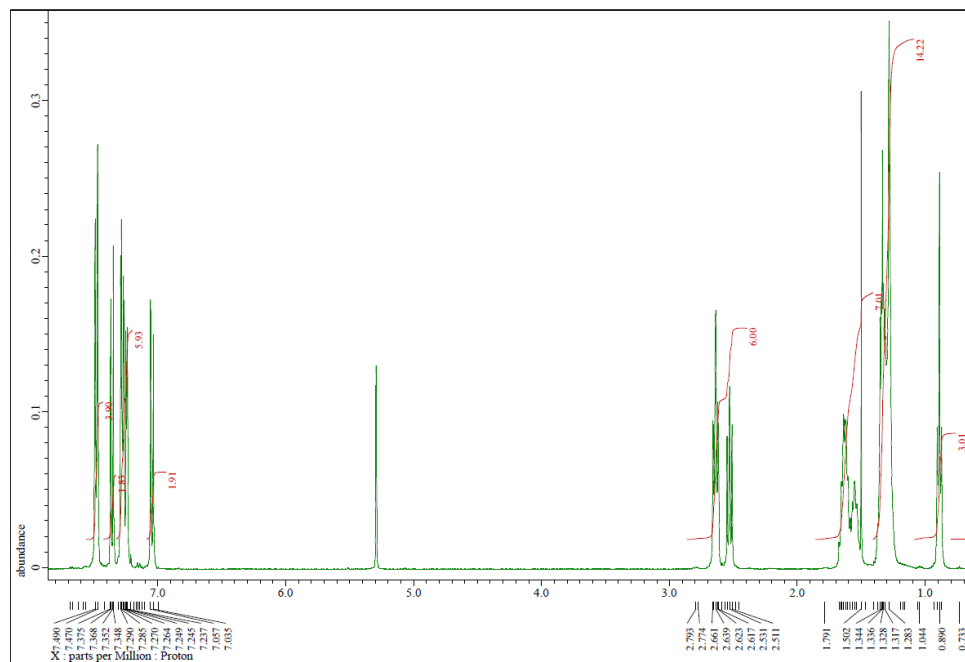


Figure S8: ^1H NMR spectrum of compound 3; 4-(9-(4-bromophenyl)nonyl)-2',3'-difluoro-4''-pentyl-1,1':4',1''-terphenyl.

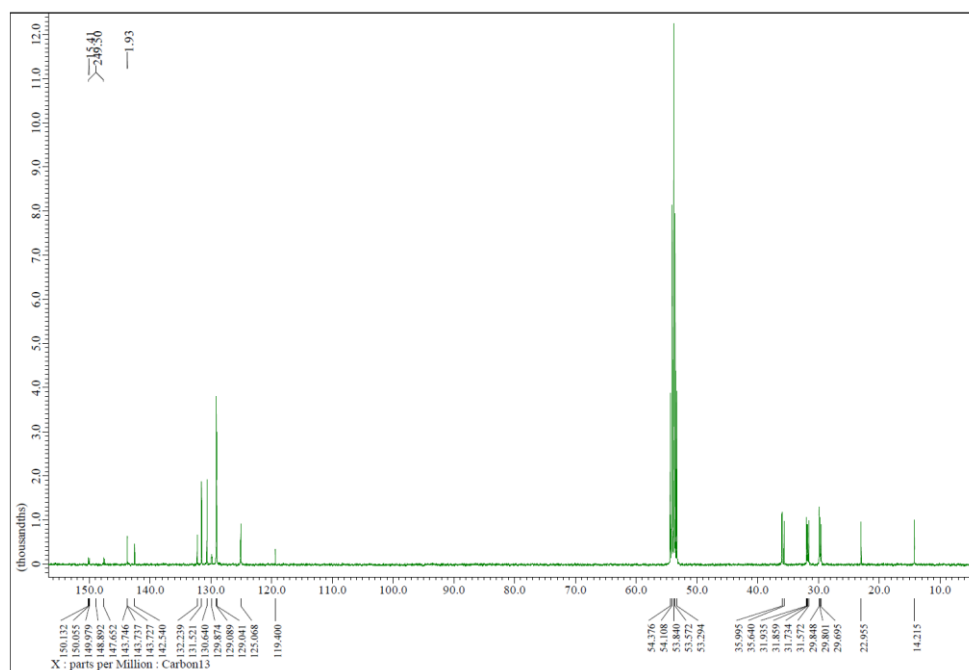


Figure S9: ^{13}C NMR spectrum of compound 3; 4-(9-(4-bromophenyl)nonyl)-2',3'-difluoro-4''-pentyl-1,1':4',1''-terphenyl.

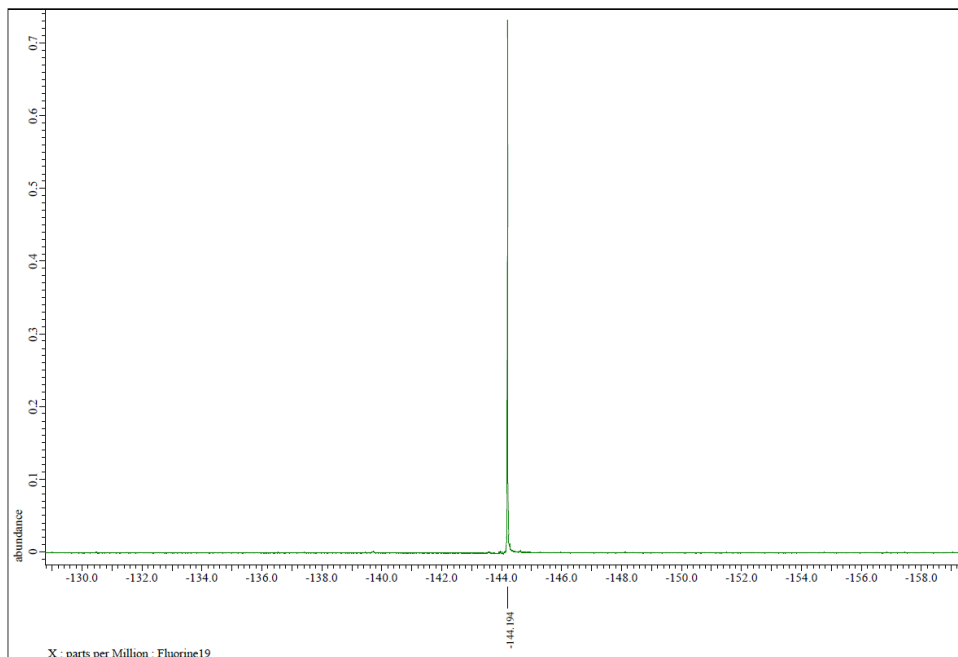


Figure S10: ^{19}F NMR spectrum of compound **3**; 4-(9-(4-bromophenyl)nonyl)-2',3'-difluoro-4''-pentyl-1,1':4',1''-terphenyl.

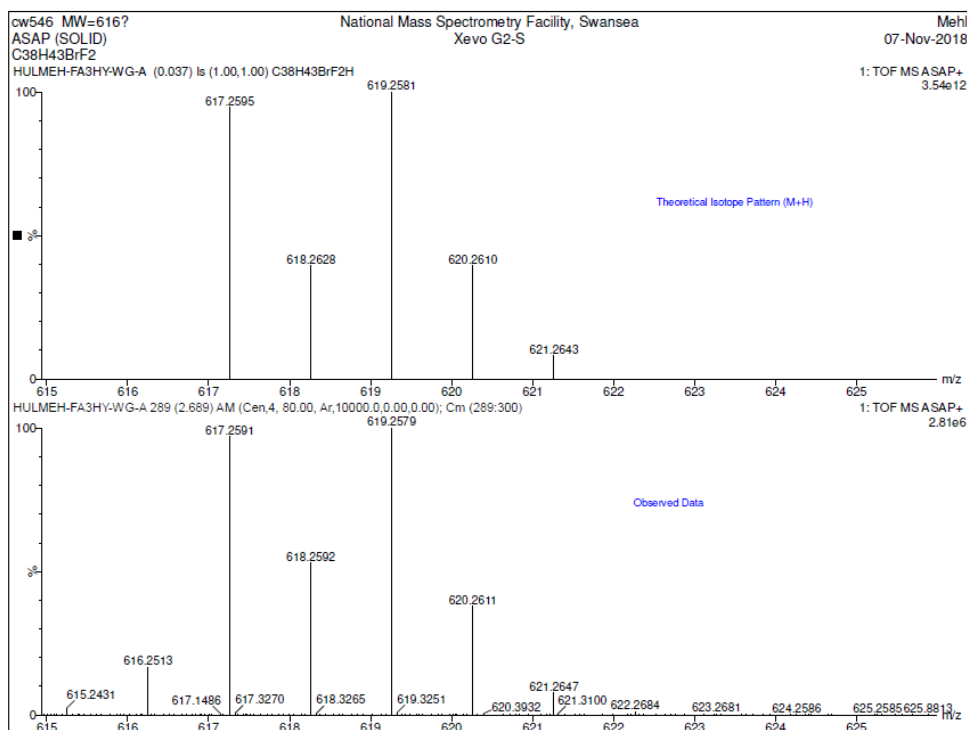


Figure S11: Top: Experimental data: high resolution mass spectrum of compound **3**; 4-(9-(4-bromophenyl)nonyl)-2',3'-difluoro-4''-pentyl-1,1':4',1''-terphenyl. Bottom: Calculated high resolution mass spectrum of compound **3**.

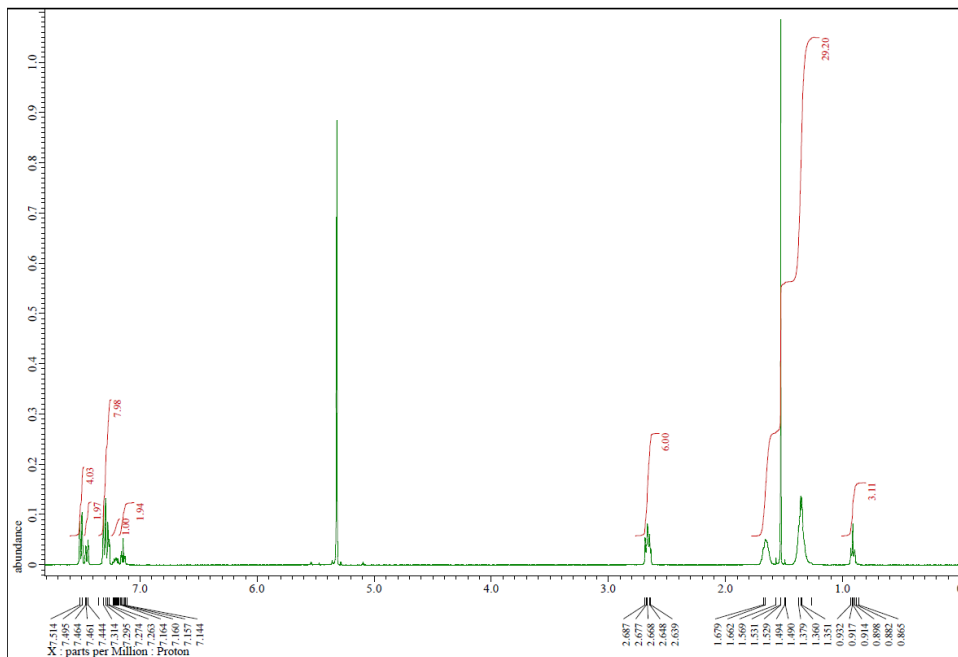


Figure S12: ^1H NMR spectrum of compound **4**; 4-(9-(2',3'-difluoro-[1,1'-biphenyl]-4-yl)nonyl)-2',3'-difluoro-4''-pentyl-1,1':4',1''-terphenyl.

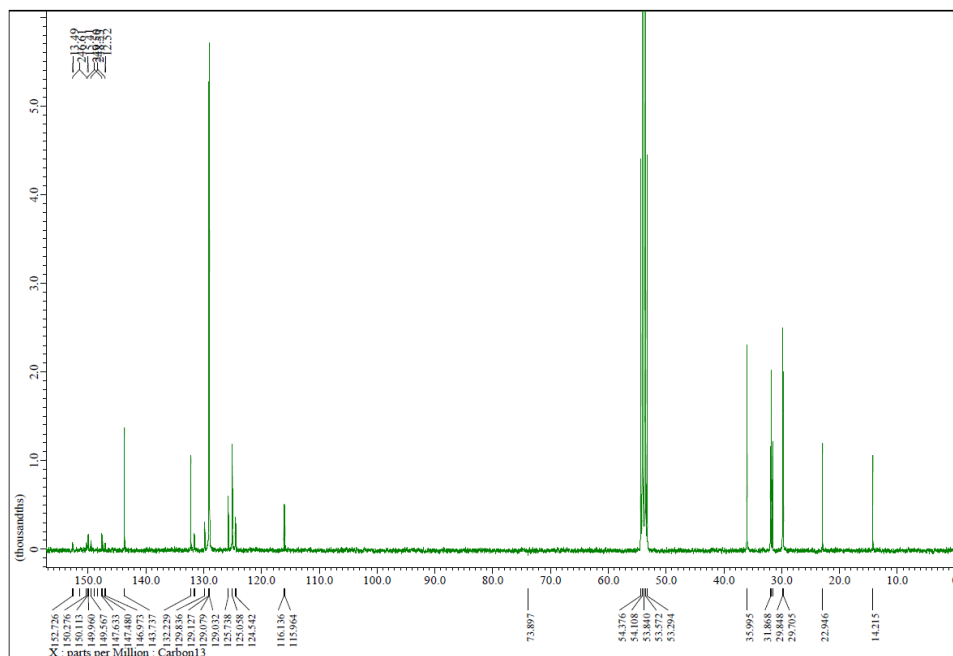


Figure S13: ^{13}C NMR spectrum of compound **4**; 4-(9-(2',3'-difluoro-[1,1'-biphenyl]-4-yl)nonyl)-2',3'-difluoro-4''-pentyl-1,1':4',1''-terphenyl.

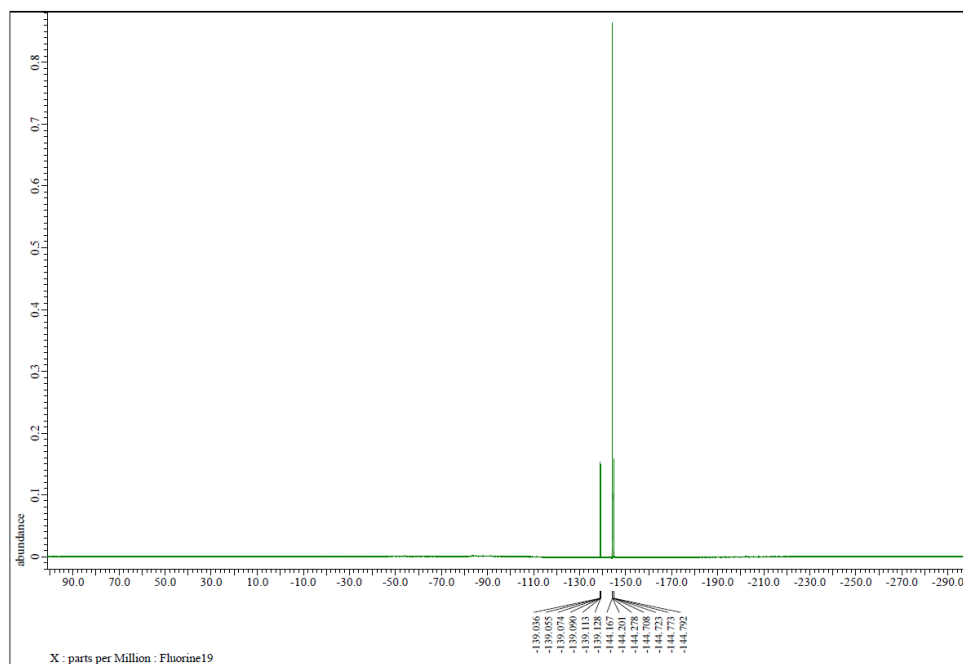


Figure S14: ^{19}F NMR spectrum of compound **4**; 4-(9-(2',3'-difluoro-[1,1'-biphenyl]-4-yl)nonyl)-2',3'-difluoro-4''-pentyl-1,1':4',1''-terphenyl

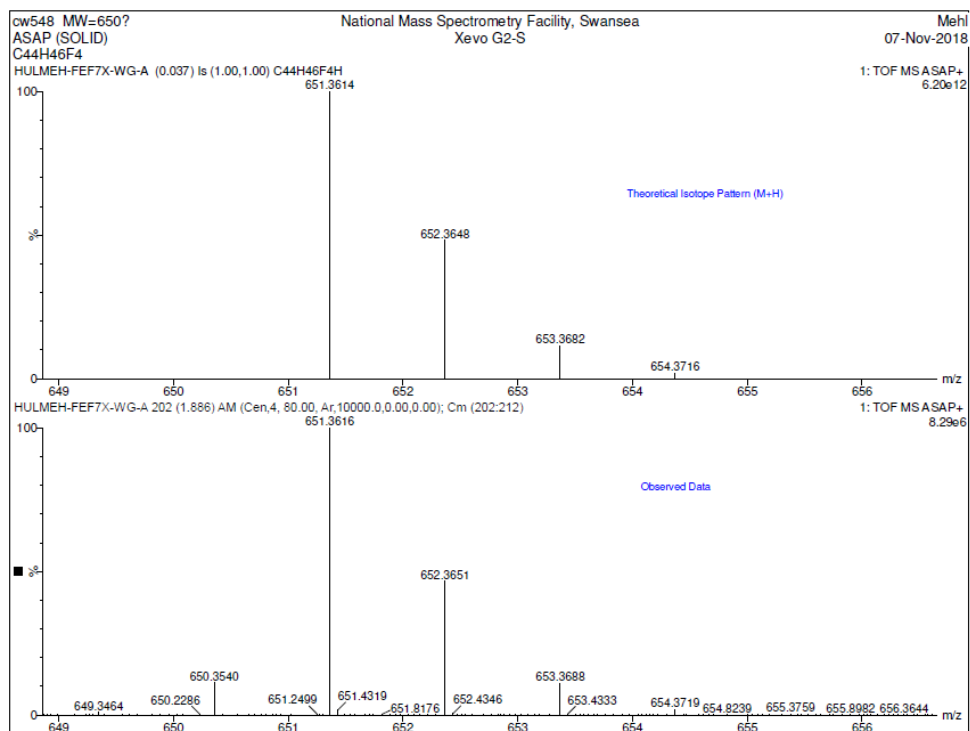


Figure S15: Top: Experimental data: high resolution mass spectrum of compound **4**; 4-(9-(2',3'-difluoro-[1,1'-biphenyl]-4-yl)nonyl)-2',3'-difluoro-4''-pentyl-1,1':4',1''-terphenyl. Bottom: Calculated high resolution mass spectrum of compound **4**.

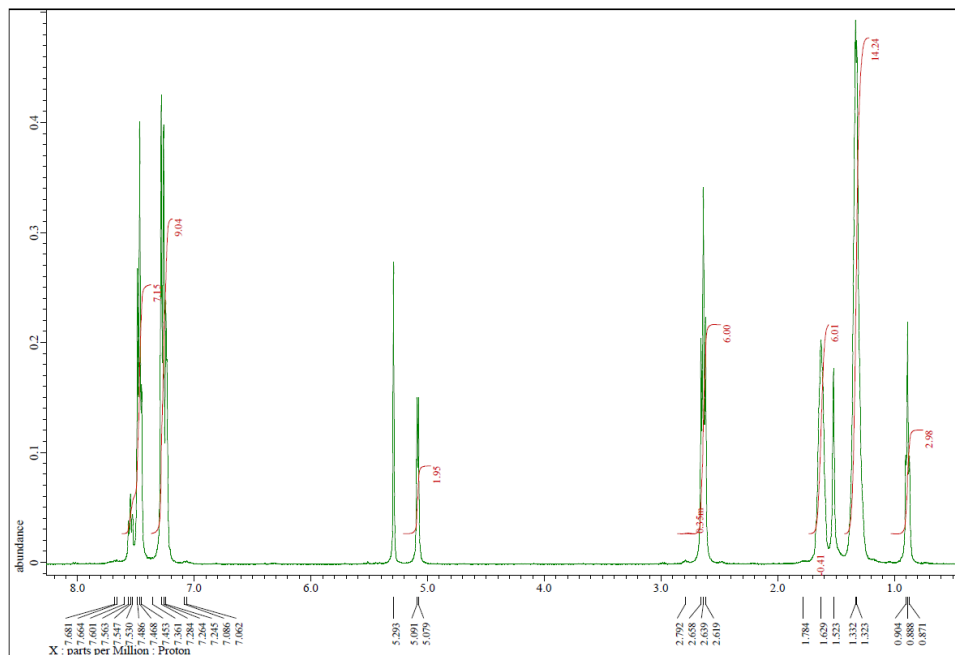


Figure S16: ^1H NMR spectrum of compound **5**; (4'-(9-(2',3'-difluoro-4''-pentyl-[1,1':4',1''-terphenyl]-4-yl)nonyl)-2,3-difluoro-[1,1'-biphenyl]-4-yl)boronic acid.

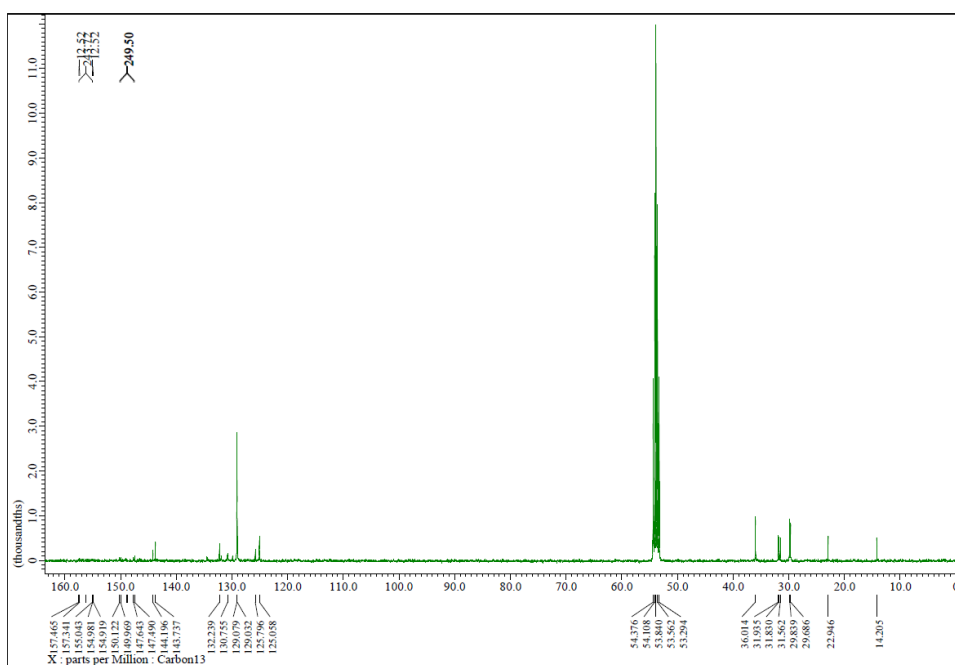


Figure S17: ^{13}C NMR spectrum of compound **5**; (4'-(9-(2',3'-difluoro-4''-pentyl-[1,1':4',1''-terphenyl]-4-yl)nonyl)-2,3-difluoro-[1,1'-biphenyl]-4-yl)boronic acid.

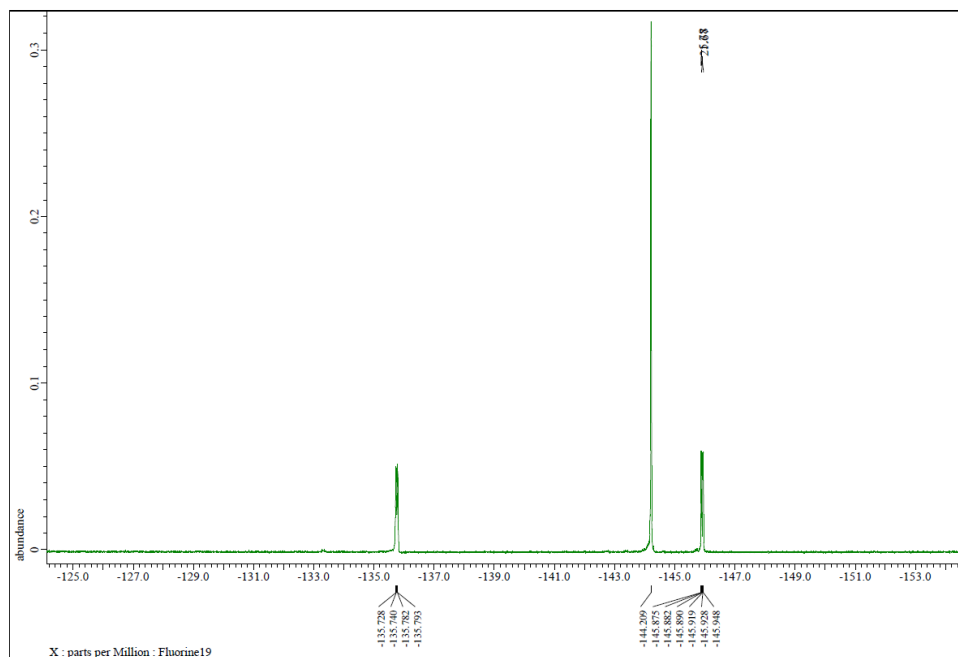


Figure S18: ^{19}F NMR spectrum of compound **5**; (4'-(9-(2',3'-difluoro-4''-pentyl-[1,1':4,1''-terphenyl]-4-yl)nonyl)-2,3-difluoro-[1,1'-biphenyl]-4-yl)boronic acid.

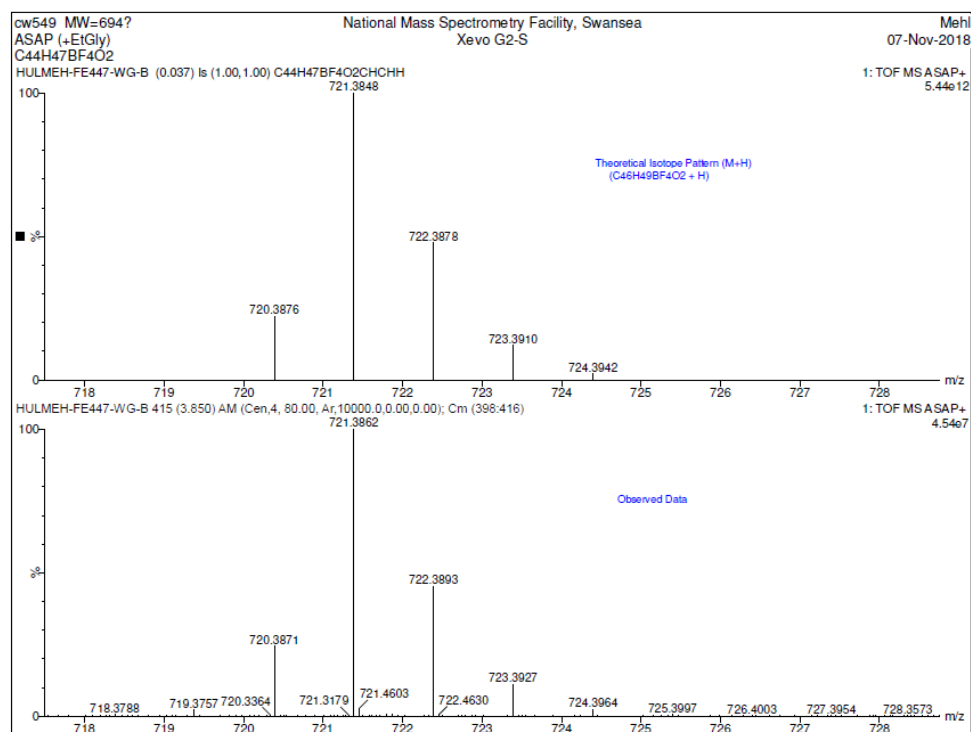


Figure S19: Top: Experimental data: high resolution mass spectrum of compound **5**; (4'-(9-(2',3'-difluoro-4''-pentyl-[1,1':4,1''-terphenyl]-4-yl)nonyl)-2,3-difluoro-[1,1'-biphenyl]-4-yl)boronic acid. Bottom: Calculated high resolution mass spectrum of compound **5**.

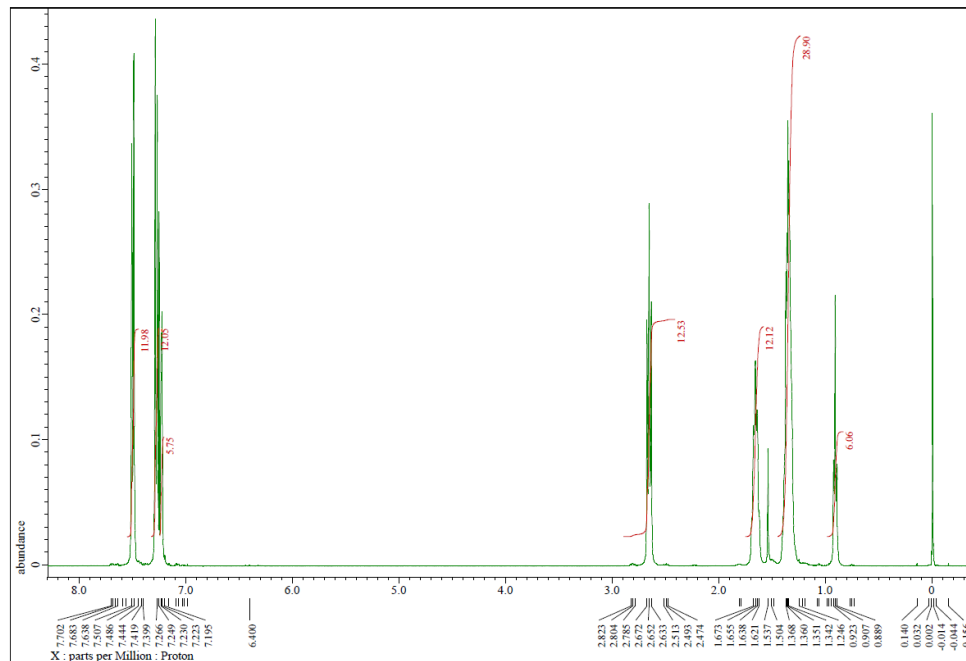


Figure S20: ^1H NMR spectrum of compound **6** (“trimer”); 4'',4''''-((2',3'-difluoro-[1,1':4,1''-terphenyl]-4,4''-diyl)bis(nonane-9,1-diyl))bis(2',3'-difluoro-4-pentyl-1,1':4,1''-terphenyl).

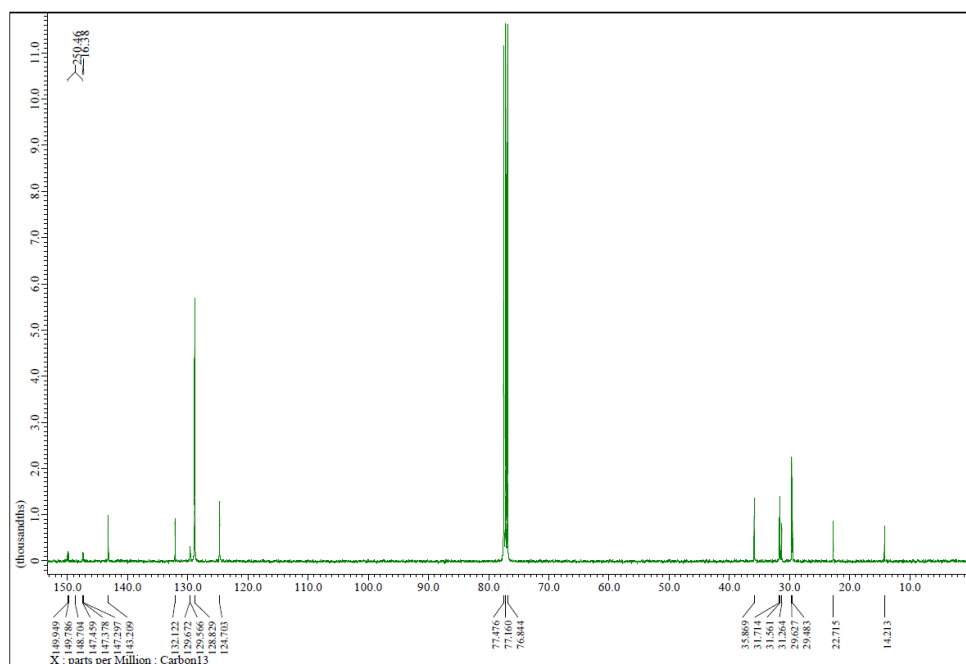


Figure S21: ^{13}C NMR spectrum of compound **6** (“trimer”); 4'',4''''-((2',3'-difluoro-[1,1':4,1''-terphenyl]-4,4''-diyl)bis(nonane-9,1-diyl))bis(2',3'-difluoro-4-pentyl-1,1':4,1''-terphenyl).

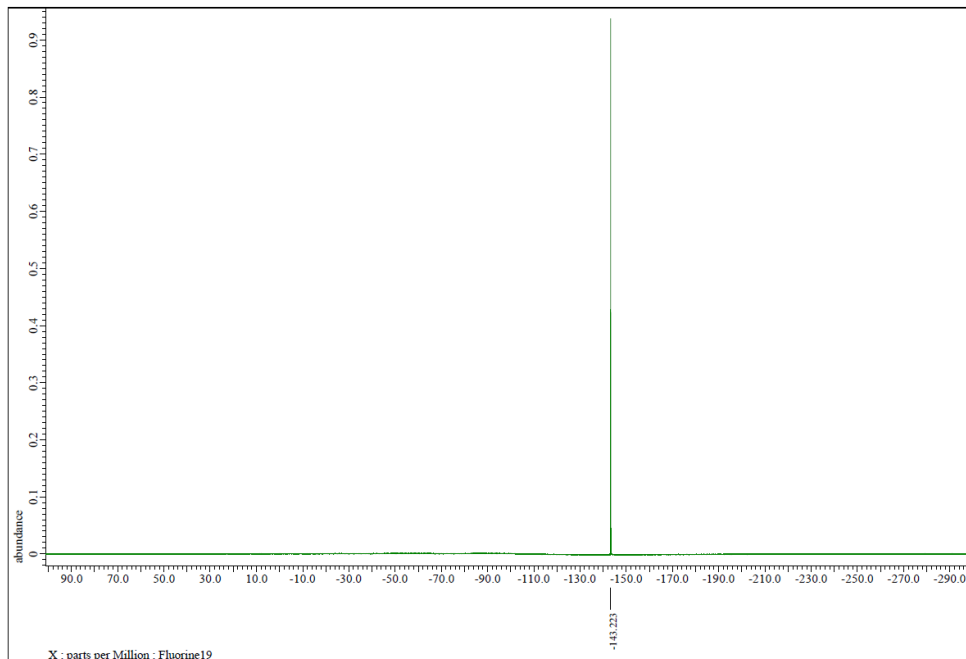


Figure S22: ^{19}F NMR spectrum of compound **6** (“trimer”); 4'',4''''-((2',3'-difluoro-[1,1':4',1''-terphenyl]-4,4''-diyl)bis(nonane-9,1-diyl))bis(2',3'-difluoro-4-pentyl-1,1':4',1''-terphenyl).

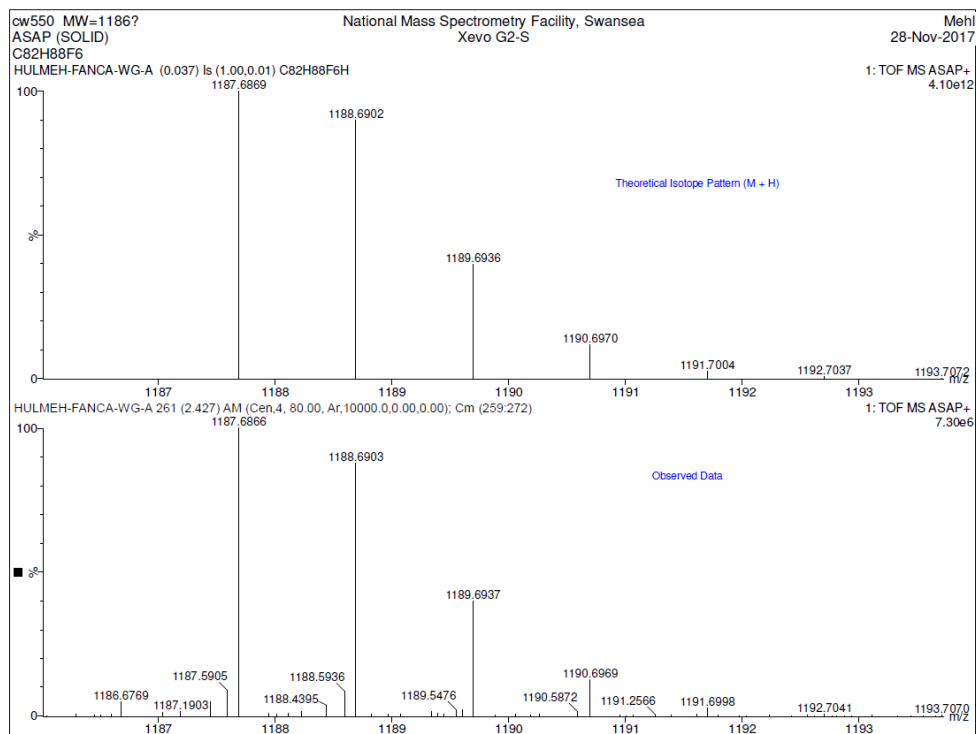


Figure S23: Top: Experimental data: high resolution mass spectrum of compound **6** (“trimer”); (4'',4''''-((2',3'-difluoro-[1,1':4',1''-terphenyl]-4,4''-diyl)bis(nonane-9,1-diyl))bis(2',3'-difluoro-4-pentyl-1,1':4',1''-terphenyl). Bottom: Calculated high resolution mass spectrum of compound **6**.

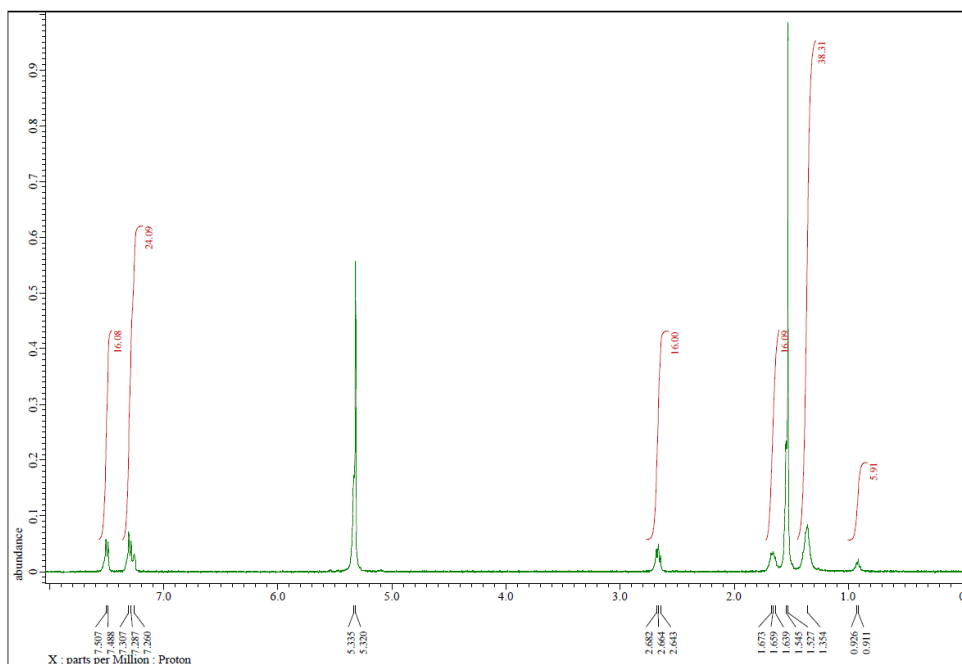


Figure S24: ^1H NMR spectrum of compound 7 (“tetramer”); 1,9-bis(4''-(9-(2',3'-difluoro-4''-pentyl-[1,1':4',1''-terphenyl]-4-yl)nonyl)-2',3'-difluoro-[1,1':4',1''-terphenyl]-4-yl)nonane.

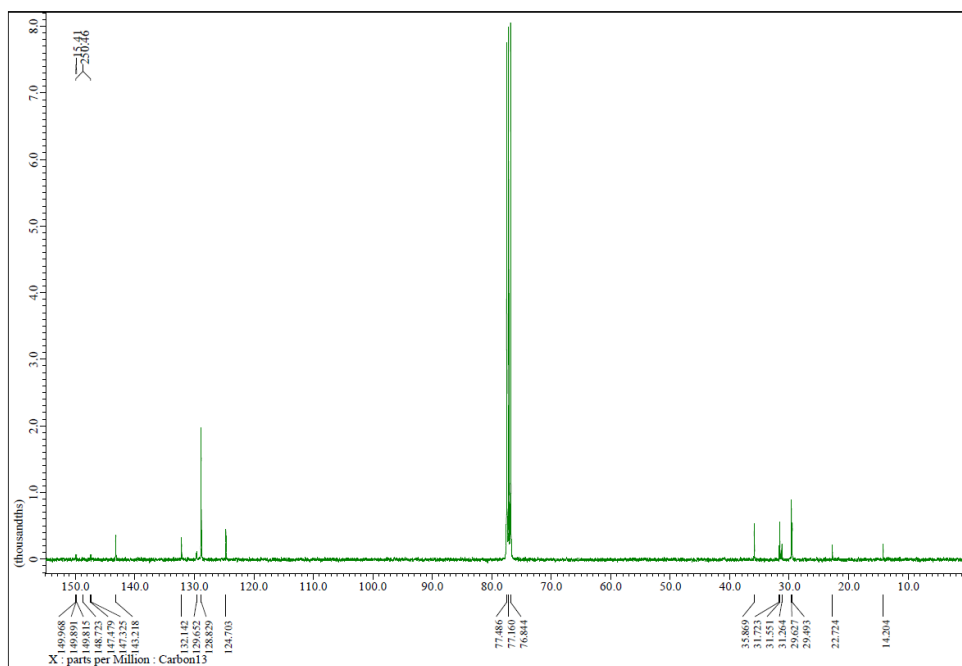


Figure S25: ^{13}C NMR spectrum of compound 7 (“tetramer”); 1,9-bis(4''-(9-(2',3'-difluoro-4''-pentyl-[1,1':4',1''-terphenyl]-4-yl)nonyl)-2',3'-difluoro-[1,1':4',1''-terphenyl]-4-yl)nonane.

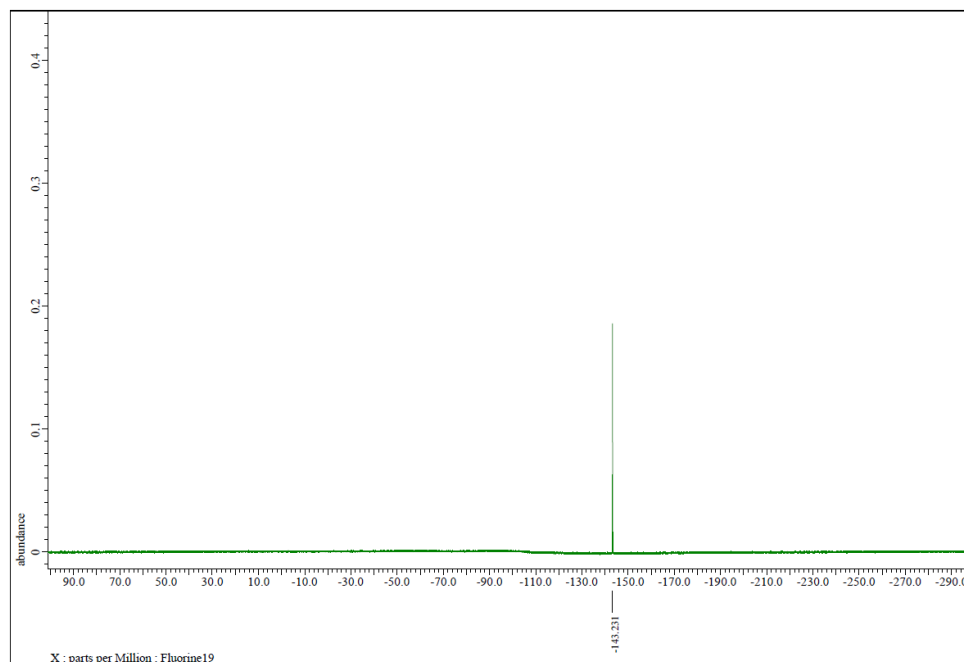


Figure S26: ^{19}F NMR spectrum of compound 7 (“tetramer”); 1,9-bis(4''-(9-(2',3'-difluoro-4''-pentyl-[1,1':4',1''-terphenyl]-4-yl)nonyl)-2',3'-difluoro-[1,1':4',1''-terphenyl]-4-yl)nonane.

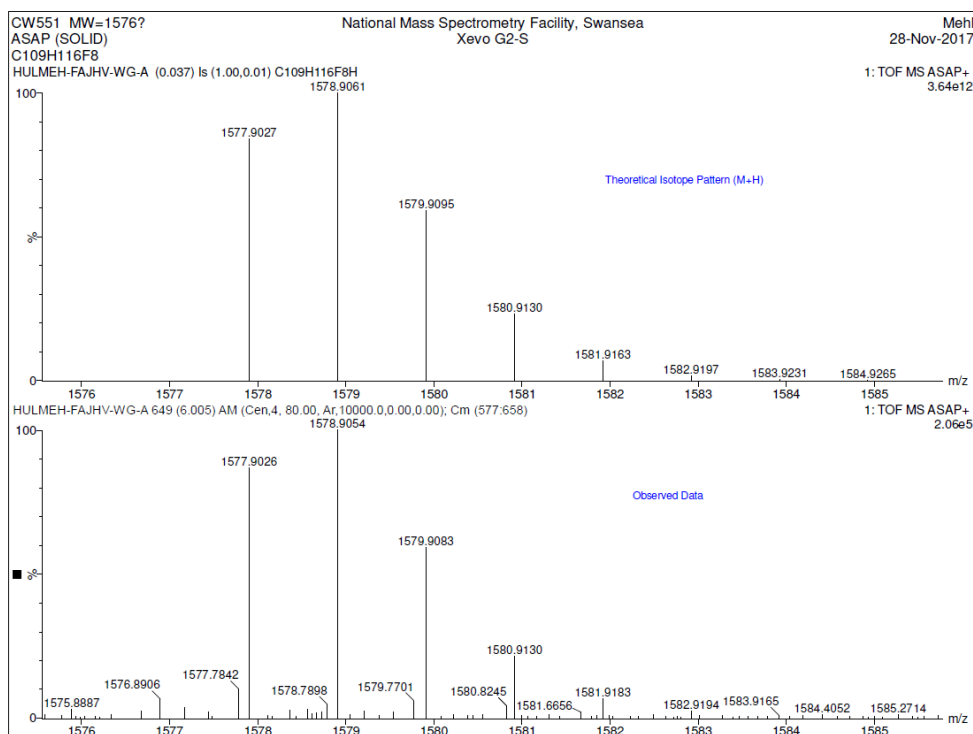


Figure S27: Top: Experimental data: high resolution mass spectrum of compound 7 (“tetramer”); 1,9-bis(4''-(9-(2',3'-difluoro-4''-pentyl-[1,1':4',1''-terphenyl]-4-yl)nonyl)-2',3'-difluoro-[1,1':4',1''-terphenyl]-4-yl)nonane. Bottom: Calculated high resolution mass spectrum of compound 7.